ADVANCED MATERIALS
www.advmat.de

Piezo-Photocatalysis over Metal–Organic Frameworks: Promoting Photocatalytic Activity by Piezoelectric Effect

Chenxi Zhang, Da Lei, Chenfan Xie, Xiaoshuai Hang, Chuanxin He, and Hai-Long Jiang**

The built-in electric field can be generated in the piezoelectric materials under mechanical stress. The resulting piezoelectric effect is beneficial to charge separation in photocatalysis. Meanwhile, the mechanical stress usually gives rise to accelerated mass transfer and enhanced catalytic activity. Unfortunately, it remains a challenge to differentiate the contribution of these two factors to catalytic performance. Herein, for the first time, isostructural metal–organic frameworks (MOFs), i.e., UiO-66-NH_2(Zr) and UiO-66-NH_2(Hf), are adopted for piezo-photocatalysis. Both MOFs, featuring the same structures except for diverse Zr/Hf-oxo clusters, possess distinctly different piezoelectric properties. Strikingly, UiO-66-NH_2(Hf) exhibits ≈2.2 times of activity compared with that of UiO-66-NH_2(Zr) under simultaneous light and ultrasonic irradiation, though both MOFs display similar activity in the photocatalytic H_2 production without ultrasonic irradiation. Given their similar pore features and mass transfer behaviors, the activity difference is unambiguously assignable to the piezoelectric effect. As a result, the contributions of the piezoelectric effect to the piezo-photocatalysis can be clearly distinguished owing to the stronger piezoelectric property of UiO-66-NH_2(Hf).

1. Introduction

Photocatalysis converts solar energy into chemical energy in an environmentally friendly way, which is considered as an effective approach to address the energy crisis and environmental pollution issues.[1] Nevertheless, the poor separation efficiency of the photogenerated electrons and holes seriously restrains the photocatalytic efficiency.[2] To reduce the recombination rate of photogenerated carriers, a variety of strategies have been developed, including defect engineering,[3] cocatalyst decoration,[4] formation of heterojunction or Z-scheme,[5] etc. Among them, the creation of built-in electric field as a driving force for charge separation has been recognized to be an effective strategy.[6] Under mechanical stretch or strain along asymmetry direction, the piezoelectric material deforms and the center of positive/negative charges in the unit-cell displace, leading to the spontaneous polarization. Accordingly, the positive and negative charges are generated on two opposite surfaces, leading to the generation of the built-in electric field. Moreover, the generated built-in electric field also induces the band bending at the solid–liquid interface, which would be further favorable to the enhancement of catalytic activity.[7] Therefore, piezo-photocatalysis, in which the piezoelectric materials are subjected to simultaneous light irradiation and mechanical stress, has become a research focus.[8]

To apply mechanical stress to piezo-(photo)catalysts, ultrasonic irradiation and mechanical stirring are the most common methods.[9] However, both methods are able to accelerate the

C. Zhang, C. He
College of Chemistry and Environmental Engineering
Shenzhen University
Shenzhen, Guangdong 518060, P. R. China
E-mail: hecx@szu.edu.cn

C. Zhang, C. Xie, H.-L. Jiang
Hefei National Laboratory for Physical Sciences at the Microscale
CAS Key Laboratory of Soft Matter Chemistry
Department of Chemistry
University of Science and Technology of China
Hefei, Anhui 230026, P. R. China
E-mail: jianglab@ustc.edu.cn

C. Zhang
Key Laboratory of Optoelectronic Devices and Systems of Ministry of Education and Guangdong Province
College of Optoelectronic Engineering
Shenzhen University
Shenzhen, Guangdong 518060, P. R. China

C. Zhang
School of Chemistry and Environmental Engineering
Hanshan Normal University
Chaozhou, Guangdong 521041, P. R. China

D. Lei
Xinjiang Key Laboratory of Explosives Safety Science
Xinjiang Technical Institute of Physics and Chemistry
Key Laboratory of Functional Materials and Devices for Special Environments
Chinese Academy of Sciences
Urumqi, Xinjiang 830011, P. R. China

X. Hang
Nanjing Institute of Environmental Sciences
Ministry of Ecology and Environment
Nanjing, Jiangsu 210042, P. R. China

The ORCID identification number(s) for the author(s) of this article can be found under https://doi.org/10.1002/adma.202106308.

DOI: 10.1002/adma.202106308

mass transfer during the reaction. As a consequence, it is a pending issue for researchers to distinguish the influence of accelerated mass transfer and piezoelectric effect on the enhancement of photocatalytic activity.[10] Unfortunately, it remains challenging to find ideal catalysts that possess similar physical and chemical properties but different piezoelectric properties, so as to understand the unique contribution of piezoelectric effect to the photocatalytic activity.

To meet this challenge, a class of crystalline porous solids, metal–organic frameworks (MOFs) featuring highly tailored and customizable structures would be promising candidates.[11] There has been a report on the piezoelectric response of MOFs, such as UiO-66-NH_2.[12] Given the MOF tunability, the metal-oxo clusters in UiO-66-NH_2 can be exchanged between Zr^{4+} and Hf^{4+} with similar physical and chemical properties, the resulting MOFs would exhibit different piezoelectric properties.[13] Furthermore, UiO-66-NH_2 has been intensively studied and exhibits great potential in photocatalysis.[14] It is assumed that the discriminative contribution between accelerated mass transfer and piezoelectric effect would be identifiable toward the improved activity in piezo-photocatalysis.

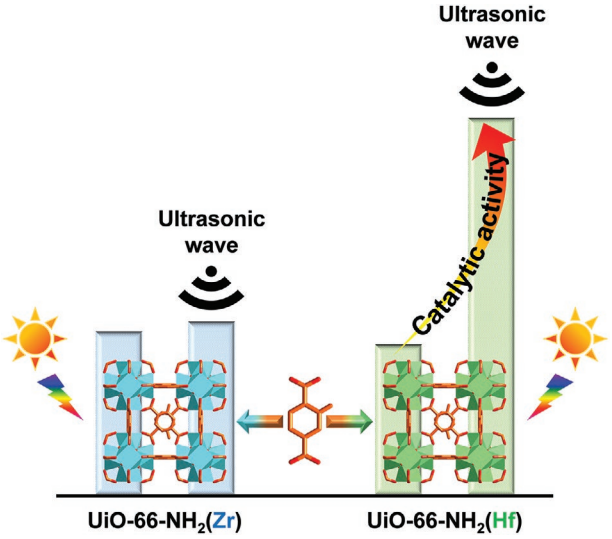

Scheme 1. Schematic H_2 production activities of UiO-66-NH_2(Zr) and UiO-66-NH_2(Hf) in photocatalysis and piezo-photocatalysis.

2. Results and Discussion

2.1. Synthesis and Characterization

With the above in mind, the isostructural MOFs, i.e., UiO-66-NH_2(Zr) and UiO-66-NH_2(Hf), which feature the same structure with different metal ions only, have been synthesized. These two MOFs display similar activities toward photocatalytic H_2 production by water splitting under common light irradiation. In sharp contrast, under simultaneous light and ultrasonic irradiation, UiO-66-NH_2(Hf) gives around 2.2 times higher activity than that of UiO-66-NH_2(Zr) (**Scheme 1**). Given similar pore sizes and structural features, both MOFs possess approximate mass transfer behaviors under ultrasonic irradiation. Accordingly, their activity difference should be attributed to their distinctly different piezoelectric responses. In addition, the influences of ultrasonic power and frequency on the activity have been investigated. To our knowledge, this is the first work on piezo-photocatalysis over MOFs.

The UiO-66-NH_2(Zr) and UiO-66-NH_2(Hf) were synthesized in a traditional solvothermal method. Powder X-ray diffraction (XRD) patterns demonstrate the success of the synthesis with good crystallinity (Figure S1, Supporting Information). According to the X-ray photoelectron spectroscopy (XPS) spectra, both Zr and Hf species are in +4 oxidation state (Figure S2a,b, Supporting Information). The Zr-MOF shows slightly higher N_2 sorption capacity and Brunauer–Emmett–Teller (BET) surface areas because of the heavier Hf than Zr element (**Figure 1**a; Figure S3, Supporting Information); they possess similar pore volume as well as pore size distribution (Table S1, Supporting Information). Both MOFs present a comparable light absorption range in the diffuse reflectance ultraviolet–visible (DR UV–vis) spectra as evidenced by similar colors (Figure 1b; Figure S4, Supporting Information). Their calculated optical bandgaps are, respectively, 2.85 and 2.86 eV, indicating their similar light harvesting ability. The water contact angles of the Zr- and Hf-MOFs are 10.6° and 12.6°, respectively (Figure S5, Supporting Information). The good hydrophilicities imply their great potential in photocatalytic H_2 production by water splitting.[15] Transmission electron microscope (TEM) and scanning electron microscope (SEM) observations suggest that the particles of both MOFs are in octahedral shape (Figure 1c,d; Figure S6, Supporting Information). Their average particle sizes are almost the same. All above results indicate that both MOFs possess similar physical and chemical properties.

2.2. Piezoelectric and Photoelectrochemical Properties

To determine the piezoelectric properties, both MOFs have been investigated by atomic force microscopy (AFM) with Kelvin probe force microscopy (KPFM) and piezoresponse force microscopy (PFM) modules. The topographic images of UiO-66-NH_2(Zr) and UiO-66-NH_2(Hf) further indicate their similar morphologies (Figure S7, Supporting Information). The surface potential images are measured in the dark and under visible light irradiation by KPFM. Under the stress of the probe tip, an inward built-in electric field forms inside UiO-66-NH_2(Hf), resulting in a positive surface voltage of up to 54.4 mV, proving its piezoelectric property (**Figure 2**a,b).[16] Interestingly, under visible light irradiation, the surface potential of UiO-66-NH_2(Hf) decreases to 41.0 mV. Owing to the influence of the inward built-in electric field, the photogenerated electrons migrate outward to the surface and then are partly depleted by the positive piezoelectric charges on the surface. The results demonstrate the formation of the built-in electric field in the catalysts, which facilitates the separation of photogenerated carriers. The similar phenomenon can be observed in UiO-66-NH_2(Zr) as well, with maximum and minimum surface

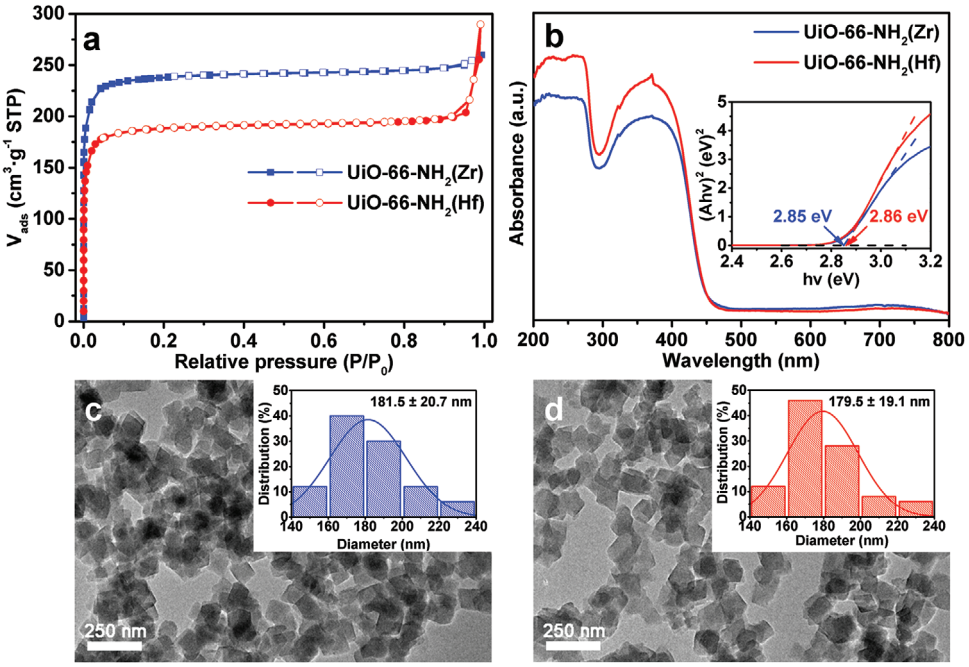

Figure 1. a) N_2 adsorption/desorption (solid/open symbols) isotherms of UiO-66-NH_2(Zr) and UiO-66-NH_2(Hf) at 77 K. b) DR UV–vis spectra of UiO-66-NH_2(Zr) and UiO-66-NH_2(Hf) (inset: Tauc plots of UiO-66-NH_2(Zr) and UiO-66-NH_2(Hf)). TEM images of c) UiO-66-NH_2(Hf) and d) UiO-66-NH_2(Zr) (inset: particle size distributions).

potentials of 27.2 and 19.0 mV, respectively (Figure S8a,b, Supporting Information). The smaller surface potential of Zr-MOF than Hf-MOF implies the weaker piezoelectric response of the former.

In the PFM measurements, under the sweep bias from −5 to 5 V, the phase changes are ≈100° and ≈180° in the piezoresponse phase hysteresis loops of UiO-66-NH_2(Zr) and UiO-66-NH_2(Hf), respectively (Figure 2c; Figure S8c, Supporting

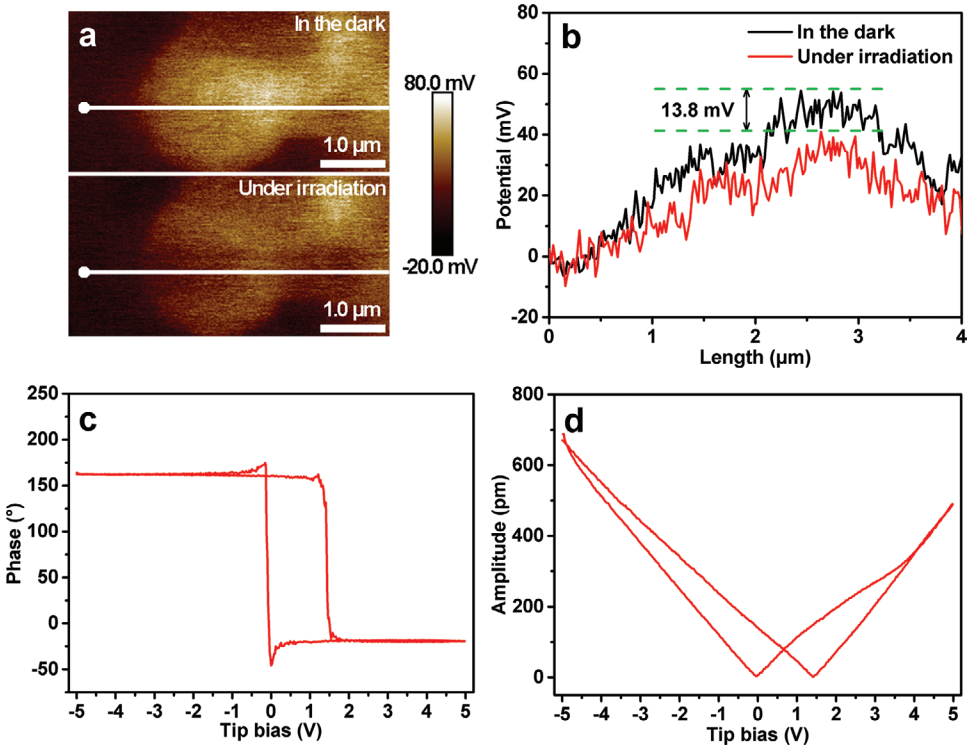

Figure 2. a) Surface potential images, b) surface potential curves, c) piezoresponse phase hysteresis loops, and d) amplitude butterfly loops of UiO-66-NH_2(Hf).

Information). The incomplete phase change of UiO-66-NH_2(Zr) indicates its weak piezoelectric intensity.[17] In the amplitude loops of the MOFs, typical butterfly shapes can be observed, but their maximum amplitudes vary greatly (Figure 2d; Figure S8d, Supporting Information). To quantitatively measure the piezoelectric intensity, the maximum effective piezoelectric coefficient d_{33} has been calculated according to the slope of the amplitude loops.[18] The d_{33} values of UiO-66-NH_2(Zr) and UiO-66-NH_2(Hf) are ≈4 and 139 pm V^{-1}, respectively. The results clarify that Hf-MOF has a much higher piezoelectric response than Zr- MOF (Figure S9, Supporting Information). The distinctly different piezoelectric effect of these two MOFs should be attributed to the larger polarity of Hf—O bond than Zr—O bond,[19] which is also supported by the previous studies.[20] To further unveil the polarity difference and reason behind the differentiated piezoelectric response between UiO-66-NH_2(Zr) and UiO-66-NH_2(Hf), their dipole moments have been evaluated by density functional theory (DFT) calculations. Considering the same linker used in both MOFs, the dipole moments of Zr/Hf-oxo cluster are analyzed for simplicity (Figure S10, Supporting Information). The dipole moment of Hf-oxo cluster is calculated to be 2.940 Debye, much higher than that of Zr-oxo cluster (1.739 Debye). The result implies that the distance between the positive and negative charge centers of UiO-66-NH_2(Hf) presents more variation under mechanical stretch or strain along asymmetry direction, resulting in the stronger spontaneous polarization and larger piezoelectric response.[16]

The common photoelectrochemical characterizations for UiO-66-NH_2(Zr) and UiO-66-NH_2(Hf) have been carried out in the absence of ultrasonic irradiation. The UiO-66-NH_2(Zr) represents a slightly higher photocurrent response (**Figure 3**a), indicating its better suppression of charge carrier recombination, which is in agreement with the intensity difference of steady-state photoluminescence (PL) emission spectra (Figure 3b). On the basis of the electrochemical impedance spectroscopy (EIS) and the fitting results (Figure 3c; Figure S11, Supporting Information), the series resistance (R_s) and the charge transfer resistance (R_{ct}) of both MOFs are nearly the same (Table S2, Supporting Information). Moreover, they exhibit similar open-circuit potential (OCP) decay curves (Figure S12a, Supporting Information), which reflect the electron migration process. Under light irradiation, the electric field intensity decreases with the photogenerated electrons and holes migrate to opposite sides. After turning off the light source, the electric field intensity increases gradually, and the OCP curve decays owing to the recombination of charge carriers. According to the calculation results, the average photogenerated carrier lifetimes of both MOFs are very close (Figure S12b, Supporting Information).[21] The Mott–Schottky measurements show that the lowest unoccupied molecular orbital (LUMO) levels of UiO-66-NH_2(Zr) and UiO-66-NH_2(Hf) are –0.64 and –0.58 V (vs NHE at pH = 7), respectively (Figure S12c,d, Supporting Information). The LUMO levels of the samples are lower than the H^+/H_2 redox potential (–0.414 V vs NHE at pH = 7), demonstrating the capability of photocatalytic H_2 production by water splitting. With their bandgap energies estimated to be 2.85 and 2.86 eV from the Tauc plots (Figure 1b), the highest occupied molecular orbital (HOMO) levels of UiO-66-NH_2(Zr) and UiO-66-NH_2(Hf) are +2.21 and +2.28 V (vs NHE at pH = 7) (Figure S13, Supporting Information). According to the linear sweep

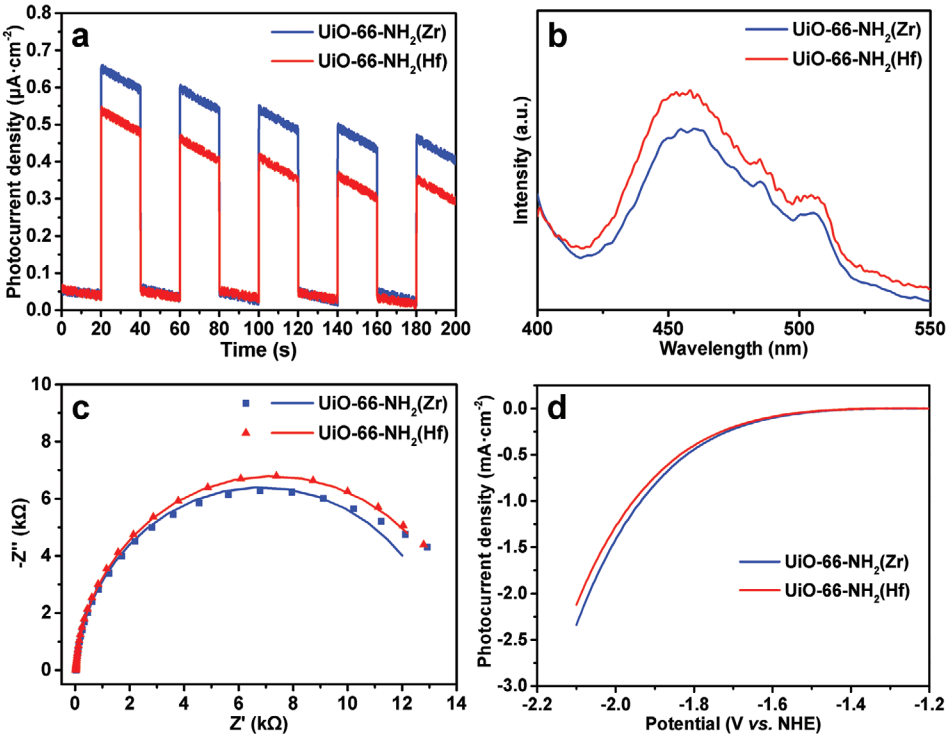

Figure 3. a) Photocurrent responses, b) PL spectra, c) EIS Nyquist plots, and d) LSV curves of UiO-66-NH_2(Zr) and UiO-66-NH_2(Hf).

voltammetry (LSV) curves recorded in the dark, the onset overpotentials of both MOFs are also similar in H_2 evolution reaction (HER) (Figure 3d). All the photoelectrochemical results reflect the negligible difference between the Zr- and Hf-MOFs in thermodynamics and kinetics.[2a]

2.3. Photocatalytic Activity

Encouraged by the above characterization results, we set out to investigate the photocatalytic H_2 production of these two MOFs with Pt nanoparticles (NPs) as the cocatalyst introduced by photodeposition. The loading amounts and the sizes of Pt NPs are fixed in both Pt/MOF composites (Table S3 and Figure S14, Supporting Information). The photocatalytic activities of the catalysts were evaluated in the optical reaction vessel (Figure S15, Supporting Information). The obtained Pt/UiO-66-NH_2(Zr) exhibits slightly higher catalytic activity than Pt/UiO-66-NH_2(Hf) under light irradiation (>380 nm, the same below) with or without stirring, which is in accordance with the better separation efficiency of photogenerated carriers in UiO-66-NH_2(Zr) (**Figure 4**a; Figure S16a,b, Supporting Information). Compared with that under light irradiation, the improved activity under simultaneous light and stirring should be ascribed to the accelerated mass transfer induced by stirring. Strikingly, under simultaneous light and ultrasonic irradiation, the activity of Pt/UiO-66-NH_2(Hf) is much improved to 1615 μmol g^{-1} h^{-1} with the apparent quantum efficiency (AQE) up to 1.60% at 380 nm, which are much higher than those of Pt/UiO-66-NH_2(Zr) (740 μmol g^{-1} h^{-1} and 0.71% at 380 nm). Given the very similar physical and chemical properties as well as pore features of both MOFs as discussed above, the mass transfer contribution to the activity should be approximate. The around 2.2 times higher activity of UiO-66-NH_2(Hf) between the two catalysts under simultaneous light and ultrasonic irradiation should be attributed to the sole factor of the larger piezoelectric effect of the Hf-MOF. Under ultrasonic irradiation, the active bubbles are generated and then collapse, resulting in high local pressure (>50 MPa).[22] Combined with the acoustic pressure generated by the ultrasonic wave, the deformation of the catalyst is induced. Therefore, polarized electric dipoles are formed in the catalyst to generate a built-in electric field. Upon simultaneous light and ultrasonic irradiation, the photogenerated electrons and holes are driven by the internal piezoelectric potential to the opposite directions/sides, accordingly improving the photocatalytic activity of Pt/UiO-66-NH_2(Hf). As a control, negligible H_2 can be detected in the absence of catalyst, demonstrating that the produced H_2 comes from the piezo-photocatalytic reaction (Figure S16c, Supporting Information).

The influence of ultrasonic power and frequency on photocatalytic activity has been further studied with Pt/UiO-66-NH_2(Hf) as the photocatalyst. When the ultrasonic power increases from 100 to 200 W with a fixed frequency of 53 kHz, the catalytic activity steadily increases (Figure 4b; Figure S16d, Supporting Information). The larger ultrasonic power would lead to greater deformation of UiO-66-NH_2(Hf) and stronger built-in electric field, which facilitates the separation of photogenerated carriers.[23] Unexpectedly, the catalytic activity decreases when

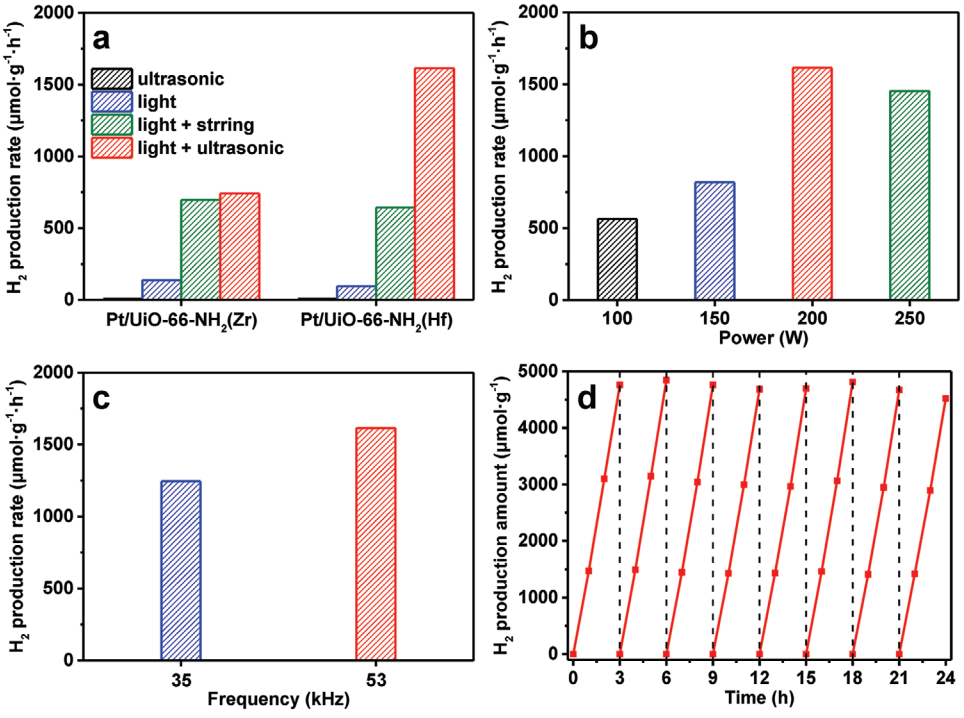

Figure 4. Photocatalytic H_2 production rates of a) Pt/UiO-66-NH_2(Zr) and Pt/UiO-66-NH_2(Hf) under different conditions, b) Pt/UiO-66-NH_2(Hf) at different ultrasonic power, and c) Pt/UiO-66-NH_2(Hf) at different ultrasonic frequencies. d) Photocatalytic H_2 production kinetic profiles of Pt/UiO-66-NH_2(Hf) in the recycling experiments under simultaneous light and ultrasonic irradiation. Unless otherwise specified, the ultrasonic power and frequency are 200 W and 53 kHz, respectively.

the ultrasonic power further improves from 200 to 250 W. It is found that the size of UiO-66-NH_2(Hf) greatly shrinks from the original 178.5 to 68.5 nm after reaction at 250 W, possibly owing to the excessive mechanical stress under such high ultrasonic power (Figure S17, Supporting Information). The results disclose the delicate balance between catalytic activity and stability in determining the ultrasonic power, providing the optimized parameter for the piezo-photocatalysis of UiO-66-NH_2(Hf). With the optimized ultrasonic power of 200 W, the Pt/UiO-66-NH_2(Hf) exhibits higher photocatalytic activity at the frequency of 53 kHz than that at 35 kHz (Figure 4c; Figure S18a, Supporting Information). It suggests that the ultrasonic frequency can alter the intensity of the applied stress and built-in electric field, and further influence the photocatalytic activity.[24] In addition, the activity of Pt/UiO-66-NH_2(Hf) does not show obvious change in the consecutive eight runs of recycling experiments (Figure 4d; Figure S18b, Supporting Information). The crystallinity and structure of the MOF, and particle sizes of the MOF and Pt, and the Pt loading amount are almost maintained after recycling reactions, manifesting the good stability of Pt/UiO-66-NH_2(Hf) catalyst (Table S3 and Figure S19, Supporting Information).

3. Conclusion

In summary, two isostructural Zr- and Hf-based MOFs, UiO-66-NH_2(M) (M = Zr, Hf), have been synthesized and investigated in piezo-photocatalysis. It is found that both MOFs present not only very similar physiochemical and photoelectrochemical properties but also negligible activity differences in photocatalytic H_2 production. By contrast, UiO-66-NH_2(Hf) exhibits 2.2 times higher activity while the activity of UiO-66-NH_2(Zr) almost remains upon further ultrasonic irradiation. In terms of their similar physical and chemical properties as well as pore features that guarantee the indiscriminate mass transfer, it is believed that the distinctly different H_2 production activity between these two MOFs under simultaneous light and ultrasonic irradiation should be attributed to the stronger piezoelectric effect of UiO-66-NH_2(Hf). Accordingly, the indistinguishable influence to piezo-photocatalysis, usually contributed by accelerated mass transfer and piezoelectric effect, can be unambiguously discriminated based on a simple and facile design in this work. As far as we know, this is not only the first report on piezo-photocatalysis over MOFs but also an unprecedented study to clearly address the contribution of the piezoelectric effect to the photocatalytic activity of piezoelectric materials.

Supporting Information

Supporting Information is available from the Wiley Online Library or from the author.

Acknowledgements

This work was supported by the National Natural Science Foundation of China (21725101, 22161142001, and 21521001) and the DNL Cooperation Fund, Chinese Academy of Sciences (DNL201911).

Conflict of Interest

The authors declare no conflict of interest.

Data Availability Statement

The data that support the findings of this study are available from the corresponding author upon reasonable request.

Keywords

metal–organic frameworks, photocatalysis, piezoelectric effect, piezo-photocatalysis

Received: August 12, 2021
Revised: September 8, 2021
Published online: October 13, 2021

[1] a) J. Ran, J. Zhang, J. Yu, M. Jaroniec, S. Z. Qiao, *Chem. Soc. Rev.* **2014**, *43*, 7787; b) Q. Wang, K. Domen, *Chem. Rev.* **2020**, *120*, 919.
[2] a) K. Sun, M. Liu, J. Pei, D. Li, C. Ding, K. Wu, H.-L. Jiang, *Angew. Chem., Int. Ed.* **2020**, *59*, 22749; b) C. Cheng, B. He, J. Fan, B. Cheng, S. Cao, J. Yu, *Adv. Mater.* **2021**, *33*, 2100317.
[3] a) Y. Zhao, Y. Zhao, R. Shi, B. Wang, G. I. N. Waterhouse, L.-Z. Wu, C.-H. Tung, T. Zhang, *Adv. Mater.* **2019**, *31*, 1806482; b) X. Ma, L. Wang, Q. Zhang, H.-L. Jiang, *Angew. Chem., Int. Ed.* **2019**, *58*, 12175; c) F. Chen, Z. Ma, L. Ye, T. Ma, T. Zhang, Y. Zhang, H. Huang, *Adv. Mater.* **2020**, *32*, 1908350.
[4] a) Q. Guo, F. Liang, X.-Y. Gao, Q.-C. Gan, X.-B. Li, J. Li, Z.-S. Lin, C.-H. Tung, L.-Z. Wu, *ACS Catal.* **2018**, *8*, 5890; b) Z. Liang, C. Qu, W. Guo, R. Zou, Q. Xu, *Adv. Mater.* **2018**, *30*, 1702891; c) M. Xu, D. Li, K. Sun, L. Jiao, C. Xie, C. Ding, H.-L. Jiang, *Angew. Chem., Int. Ed.* **2021**, *60*, 16372; d) S. Yang, D. Fan, W. Hu, B. Pattengale, C. Liu, X. Zhang, J. Huang, *J. Phys. Chem. C* **2018**, *122*, 3305.
[5] a) G. Xu, H. Zhang, J. Wei, H.-X. Zhang, X. Wu, Y. Li, C. Li, J. Zhang, J. Ye, *ACS Nano* **2018**, *12*, 5333; b) P. Hu, R. Wang, Z. Gao, S. Jiang, Z. Zhao, H. Ji, Z. Zhao, *Appl. Catal., B* **2021**, *296*, 120371; c) J. Bian, Z. Zhang, J. Feng, M. Thangamuthu, F. Yang, L. Sun, Z. Li, Y. Qu, D. Tang, Z. Lin, F. Bai, J. Tang, L. Jing, *Angew. Chem., Int. Ed.* **2021**, *60*, 20906; d) M. Zhang, M. Lu, Z.-L. Lang, J. Liu, M. Liu, J.-N. Chang, L.-Y. Li, L.-J. Shang, M. Wang, S.-L. Li, Y.-Q. Lan, *Angew. Chem., Int. Ed.* **2020**, *59*, 6500.
[6] a) Y. Guo, W. Shi, Y. Zhu, *EcoMat* **2019**, *1*, e12007; b) X. Chen, J. Wang, Y. Chai, Z. Zhang, Y. Zhu, *Adv. Mater.* **2021**, *33*, 2007479; c) H. Ben, Y. Liu, X. Liu, X. Liu, C. Ling, C. Liang, L. Zhang, *Adv. Funct. Mater.* **2021**, *31*, 2102315.
[7] a) F. Chen, H. Huang, L. Guo, Y. Zhang, T. Ma, *Angew. Chem., Int. Ed.* **2019**, *58*, 10061; b) C. Hu, S. Tu, N. Tian, T. Ma, Y. Zhang, H. Huang, *Angew. Chem., Int. Ed.* **2021**, *60*, 16309.
[8] a) Y. Yu, X. Wang, *Adv. Mater.* **2018**, *30*, 1800154; b) L. Guo, C. Zhong, J. Cao, Y. Hao, M. Lei, K. Bi, Q. Sun, Z. L. Wang, *Nano Energy* **2019**, *62*, 513; c) S. Tu, Y. Guo, Y. Zhang, C. Hu, T. Zhang, T. Ma, H. Huang, *Adv. Funct. Mater.* **2020**, *30*, 2005158.
[9] a) Y. Feng, H. Li, L. Ling, S. Yan, D. Pan, H. Ge, H. Li, Z. Bian, *Environ. Sci. Technol.* **2018**, *52*, 7842; b) W. Tong, Y. Zhang, H. Huang, K. Xiao, S. Yu, Y. Zhou, L. Liu, H. Li, L. Liu, T. Huang, M. Li, Q. Zhang, R. Du, Q. An, *Nano Energy* **2018**, *53*, 513; c) J. Ling, K. Wang, Z. Wang, H. Huang, G. Zhang, *Ultrason. Sonochem.* **2020**, *61*, 104819.
[10] L. Pan, S. Sun, Y. Chen, P. Wang, J. Wang, X. Zhang, J.-J. Zou, Z. L. Wang, *Adv. Energy Mater.* **2020**, *10*, 2000214.

[11] a) H. Furukawa, K. E. Cordova, M. O'Keeffe, O. M. Yaghi, *Science* **2013**, *341*, 1230444; b) H.-C. J. Zhou, S. Kitagawa, *Chem. Soc. Rev.* **2014**, *43*, 5415; c) B. Li, H.-M. Wen, Y. Cui, W. Zhou, G. Qian, B. Chen, *Adv. Mater.* **2016**, *28*, 8819; d) T. Islamoglu, S. Goswami, Z. Li, A. J. Howarth, O. K. Farha, J. T. Hupp, *Acc. Chem. Res.* **2017**, *50*, 805; e) A. Dhakshinamoorthy, Z. Li, H. Garcia, *Chem. Soc. Rev.* **2018**, *47*, 8134; f) L. Jiao, Y. Wang, H.-L. Jiang, Q. Xu, *Adv. Mater.* **2018**, *30*, 1703663; g) H. Li, L. Li, R.-B. Lin, W. Zhou, Z. Zhang, S. Xiang, B. Chen, *EnergyChem* **2019**, *1*, 100006; h) Y.-Z. Li, Z.-H. Fu, G. Xu, *Coord. Chem. Rev.* **2019**, *388*, 79; i) E. D. Kinigstein, J. Zhang, X. Zhang, C. A. Schmuttenmaer, J. Huang, *J. Am. Chem. Soc.* **2020**, *142*, 21050.

[12] Y. Sun, J. Gao, Y. Cheng, Y.-W. Zhang, K. Zeng, *J. Phys. Chem. C* **2019**, *123*, 3122.

[13] Z. Hu, Y. Wang, D. Zhao, *Chem. Soc. Rev.* **2021**, *50*, 4629.

[14] a) C. G. Silva, I. Luz, F. X. Llabrés i Xamena, A. Corma, H. García, *Chem. - Eur. J.* **2010**, *16*, 11133; b) D. Sun, W. Liu, M. Qiu, Y. Zhang, Z. Li, *Chem. Commun.* **2015**, *51*, 2056; c) J.-D. Xiao, Q. Shang, Y. Xiong, Q. Zhang, Y. Luo, S.-H. Yu, H.-L. Jiang, *Angew. Chem., Int. Ed.* **2016**, *55*, 9389; d) F.-M. Zhang, J.-L. Sheng, Z.-D. Yang, X.-J. Sun, H.-L. Tang, M. Lu, H. Dong, F.-C. Shen, J. Liu, Y.-Q. Lan, *Angew. Chem., Int. Ed.* **2018**, *57*, 12106.

[15] S. Zhang, G. Cheng, L. Guo, N. Wang, B. Tan, S. Jin, *Angew. Chem., Int. Ed.* **2020**, *59*, 6007.

[16] C. Hu, F. Chen, Y. Wang, N. Tian, T. Ma, Y. Zhang, H. Huang, *Adv. Mater.* **2021**, *33*, 2101751.

[17] D. Yu, Z. Liu, J. Zhang, S. Li, Z. Zhao, L. Zhu, W. Liu, Y. Lin, H. Liu, Z. Zhang, *Nano Energy* **2019**, *58*, 695.

[18] C. Hu, H. Huang, F. Chen, Y. Zhang, H. Yu, T. Ma, *Adv. Funct. Mater.* **2020**, *30*, 1908168.

[19] Y. Sun, Z. Hu, D. Zhao, K. Zeng, *Nanoscale* **2017**, *9*, 12163.

[20] a) M. H. Beyzavi, R. C. Klet, S. Tussupbayev, J. Borycz, N. A. Vermeulen, C. J. Cramer, J. F. Stoddart, J. T. Hupp, O. K. Farha, *J. Am. Chem. Soc.* **2014**, *136*, 15861; b) W. Zheng, K. H. Bowen, J. Li, I. Dąbkowska, M. Gutowski, *J. Phys. Chem. A* **2005**, *109*, 11521.

[21] a) D. Li, S.-H. Yu, H.-L. Jiang, *Adv. Mater.* **2018**, *30*, 1707377; b) G. Yang, S. Li, X. Wang, B. Ding, Y. Li, H. Lin, D. Tang, X. Ren, Q. Wang, S. Luo, J. Ye, *Appl. Catal., B* **2021**, *297*, 120268.

[22] a) E. B. Flint, K. S. Suslick, *Science* **1991**, *253*, 1397; b) J. Wu, N. Qin, D. Bao, *Nano Energy* **2018**, *45*, 44; c) O. Amiri, K. Salar, P. Othman, T. Rasul, D. Faiq, M. Saadat, *J. Hazard. Mater.* **2020**, *394*, 122514; d) X. Li, W. Wang, F. Dong, Z. Zhang, L. Han, X. Luo, J. Huang, Z. Feng, Z. Chen, G. Jia, T. Zhang, *ACS Catal.* **2021**, *11*, 4739.

[23] M. Wang, Y. Zuo, J. Wang, Y. Wang, X. Shen, B. Qiu, L. Cai, F. Zhou, S. P. Lau, Y. Chai, *Adv. Energy Mater.* **2019**, *9*, 1901801.

[24] J. Ma, J. Ren, Y. Jia, Z. Wu, L. Chen, N. O. Haugen, H. Huang, Y. Liu, *Nano Energy* **2019**, *62*, 376.